Multiscale Structural Characterization of Biobased Diallyl–Eugenol Polymer Networks

Agustín Rios de Anda, Paul Sotta, Tina Modjinou, Valérie Langlois, Davy-Louis Versace, Estelle Renard

Multiscale Structural Characterization of Bio-based Diallyl-Eugenol Polymer Networks

Agustín Rios de Anda,*,† Paul Sotta,‡ Tina Modjinou,† Valérie Langlois,† Davy-Louis Versace,† and Estelle Renard†

†*Institut de Chimie et des Matériaux Paris-Est - Université Paris-Est Créteil, UMR 7182 CNRS, 2 rue Henri Dunant, 94320, Thiais, France*

‡*Laboratoire Polymères et Matériaux Avancés, UMR 5268 CNRS-Solvay, Solvay in Axel'One, 87 rue des Freres Perret, 69192, Saint Fons, France*

E-mail: rios@icmpe.cnrs.fr

Phone: +33 (0)1 49 78 12 28

Abstract

Biosourced eugenol-based polymer networks have a potential functionality for antibacterial coating applications. The presence of carvacrol, a phenol compound, exacerbates these properties. However, the relationship between the network structure and the macroscopic thermomechanical behavior is not known for these biopolymers. Thus, this work details a robust study of this relationship through a multiscale experimental approach combining Dielectric spectroscopy, DMA, Tensile testing and Time domain $DQ\ ^1H$ NMR. It was shown that carvacrol has an influence on the molecular mobility of the materials. Namely it induces the appearance of a shouldering on the γ relaxation and a diminishing of T_α. More surprisingly, up to $20\%_{wt}$, carvacrol increases the elastic E' and Young's E moduli. This observation can be interpreted as an increase of the crosslink density ν_C of the networks. Time domain $DQ\ ^1H$ NMR shows that the

residual dipolar coupling constant D_{res} also increases. Thus, carvacrol seems to act as both a thermal plasticizer and a mechanical reinforcement, which may seem to be antagonistic trends. For carvacrol contents over $20\%_{wt}$ these properties diminish due to a saturation of this molecule in the networks and the onset of a phase separation. By combining the aforementioned techniques, it was proven that carvacrol linearly increased the measured crosslink density and thermomechanical properties by physically bonding to the networks through $\pi - \pi$ interactions. These interactions would act as physical crosslinks. This work demonstrates that by correlating the results of various multiscale experimental techniques, a better comprehension of the structure-property relationship can be established for biobased functional polymer networks.

Introduction

For the past several years, research on biosourced polymers has had a great rise in interest among the scientific and industrial communities[1–4] One of the main aims of this interest is to replace petrosourced materials in everyday usage, more specifically, engineered biosourced polymers are starting to find their way into technical applications.[1–4] One example of such materials are antibacterial coatings based on biosourced monomers which have been recently developed,[5–8] notably *eugenol*-based polymeric networks.[6–8] These materials are obtained by UV-curing, which allows a rapid crosslinking kinetics and avoids using harmful solvents. To enhance their antibacterial behavior, biosourced additives such as *carvacrol* can be added to the formulation. It was shown that the addition of this molecule exacerbated the antibacterial effect of eugenol-based coatings when in contact with *Escherichia coli* and *Staphylococcus aureus*.[8] Specifically, networks were fully effective against these bacteria for carvacrol contents over $20\%_{wt}$.

As promising technical materials, the functional macroscopic behavior of these eugenol-based polymeric networks, namely their thermomechanical properties have to be thoroughly characterized. This paper thus presents a multiscale investigation of the relationship between

the network structure, the molecular mobility, and the macroscopic thermomechanical properties of eugenol-based networks containing various carvacrol concentrations. As such, the proposed approach combines the use of Broadband Dielectric Spectroscopy (BDS), Dynamic Mechanical Analysis (DMA), Tensile testing, and Time domain $DQ\ ^1H$ NMR to achieve a full multiscale characterization of these anti-bacterial biobased networks.

The molecular mobility of the studied materials, namely their main and secondary relaxations, was studied by BDS and DMA. The secondary and main relaxations can be easily identified by BDS. The activation energies of these relaxations can be also readily obtained, which contributes to elucidate the involved molecular motions.[9–11] Moreover DMA measurements made possible to evaluate the influence of carvacrol on the main molecular relaxation as well as on the mechanical elastic modulus as a function of temperature.[12–14] Tensile tests at high temperatures complemented these characterizations so as to obtain a mechanical measurement of the crosslink density of each of the studied networks in the elastomeric regime (*i.e.* well above T_g). These measurements were aimed to study the influence of the crosslinking agent and that of carvacrol on the network structure and hence on the thermomechanical behavior of the eugenol-based networks.

The network architecture was then characterized by ^1H Double Quantum (DQ) Time domain NMR. This technique has been proven successful to characterize the intrinsic morphology of crosslinked elastomeric-like materials such as natural and synthetic rubbers, PDMS and other elastomers, as well as the influence of chemical modifications, variation of crosslink density and aging on such materials.[15–34] Recently, this technique was successfully used in combination with DMA measurements to study the relationship between the structure of Poly(trimethylene carbonate) (PTMC) and their macroscopic thermomechanical behavior.[35]

This robust combination of multiscale techniques has opened the perspective of obtaining a fine characterization of crosslinked polymeric networks with different chemical structures. Thus, this work aims to demonstrate that such an approach allows yet a better understanding of the relationship between the structure and the thermomechanical behavior of biosourced

eugenol-based polymer networks with carvacrol-enhanced antibacterial properties.

Materials

Chemicals and reactants

Eugenol (99% Alfa Aesar) and Allylbromide (99% Sigma Aldrich) were used to synthesize diallyl-eugenol (hereafter named ***AE***) following the same protocol as Renard *et.al.*[6–8] To obtain the polymer networks, two thiolene-based crosslinking agents were used: trimethylolpropane tris(3-mercaptopropionate) (≥95% Sigma Aldrich - ***3T***) and pentaerythritol tetrakis(3-mercaptopropionoate) (≥95% Sigma Aldrich - ***4T***). 2,2-Dimethoxy-2-phenylacetatophenone (99% Sigma Aldrich - ***DMPA***) was used as a photo-induced initiator.

Preparation of *AE-3T/4T+CV* polymeric networks

In order to prepare AE-based networks,[6–8] 400 mg of **AE** were poured in silicon molds measuring 2.5x5x0.75cm^3. $3T$ and $4T$ crosslinking agents were added in stoichiometric quantities so as to have one double bond of AE per thiol function in the reaction medium. As such, either 520mg of $3T$ or 480mg of $4T$ were added to the silicon molds. The appropriate amounts of CV were introduced in the AE-based networks as follows. Four percentages were studied: 5, 10, 20 and 30%$_{wt}$. Finally 232 μl of a solution of DMPA in acetone at a concentration of 100g/l (corresponding to 5%wt of DMPA as regards to the AE content) was poured into the molds. The precursors were carefully mixed, then each mold was placed in an oven at 70°C for 45 minutes so as to evaporate the acetone and allow a better mixing of the monomers. Afterwards, the medium was degassed for 15 minutes under vacuum at room temperature. Lastly, the photo-polymerization was undertaken. Each mold was placed under a L8251 Hamamatsu LC8 UV polychromatic lamp (between 250 and 450 nm) held at a height of 11cm for 10 minutes at room temperature. The power of the lamp at this distance was measured to be 180 mW/cm^2. Figure 1 shows the chemical structure of the

neat *AE-3T* and *AE-4T* polymeric networks.

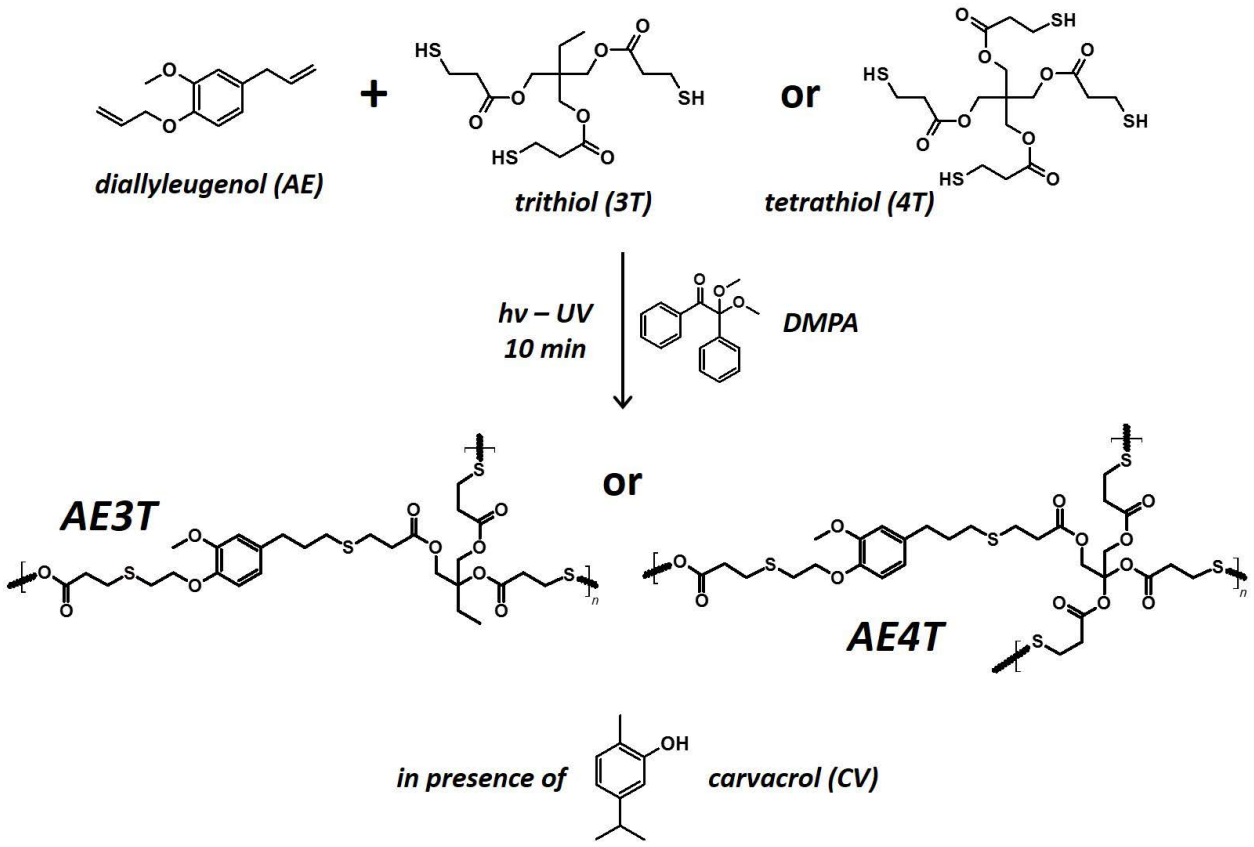

Figure 1: Molecular structures of the obtained neat (a) *AE-3T* and (b) *AE-4T* networks.

Previous works have successfully shown that this experimental procedure yields completely crosslinked films where all monomers have effectively reacted.[6–8] This was rapidly verified herein by FT-IR Spectroscopy (Brucker Tensor 27 - ATR, 32 scans) on an unreacted medium as well as on the Neat *AE-3T* and *AE-4T* networks. Figure SI.1 (*Support Information*) shows that the peak at 2568 cm^{-1}, corresponding to the SH[6–8] function disappear for the Neat *AE-3T* and *AE-4T* networks, meaning that these functions have completely reacted, forming a network..

It is important to note herein that the chemical structures of the obtained networks are fundamentally the same, the sole differences are the functionality and the density of the crosslinks. Indeed, *3T* yields a trifunctional network whereas *4T* gives a tetrafunctional one. For 100% reacted networks with perfect topologies, the stoichiometric crosslink density

would then be 1.56×10^{-3} mol/g for *AE-3T* and 1.17×10^{-3} mol/g for *AE-4T* (*i.e.* a 4/3 ratio between both networks) with the *AE-3T* network being more crosslinked in theory. Measured or estimated experimental values shall be later on discussed in reference with those values.

Experimental techniques

Broadband Dielectric Spectroscopy Measurements

Dielectric measurements were performed on a Novocontrol BDS Alpha Analyzer equipped with a Quatro temperature control system. 900 μm-thick samples were cut in disks of diameter 2cm and were placed in between gold-plated electrodes. The electric field voltage was fixed at 3V AC. Data was acquired from -150 to 70°C with 4°C steps. Each temperature step was scanned at 41 frequencies ranging from 0.01 to 10^6 Hz. The software WinFit from Novocontrol was used to analyze the 3D plot data allowing the identification and study of the secondary and main molecular relaxations as a function of temperature and frequency.

The obtained complex permittivity ϵ^* data was fitted for each studied sample. For the secondary relaxations corresponding to local motions within the polymer chains (*i.e.* β, γ, δ, ...), the Cole-Cole model described in Equation 1 was used.[10,11]

$$\epsilon^* = \epsilon' + i\epsilon'' = \epsilon_\infty + \frac{\epsilon_S - \epsilon_\infty}{1 + (i\omega\tau)^m} \tag{1}$$

where ω is the angular frequency, τ the relaxation time, m is an exponent describing the broadening of the molecular relaxations ($0 < m < 1$), ϵ', ϵ'', are the real and loss permittivities, and ϵ_S and ϵ_∞ are the "static" and "infinite frequency" dielectric constants respectively.

In the case of the main α relaxation, the Havriliak-Negami model detailed in Equation 2[10,11,36] was utilized.

$$\epsilon^* = \epsilon' + i\epsilon'' = \epsilon_\infty + \frac{\epsilon_S - \epsilon_\infty}{\left(1 + (i\omega\tau)^m\right)^n} \quad (2)$$

This model takes into account that main α relaxations have an asymmetric relaxation time τ distribution when compared to secondary relaxations. Such asymmetry is described by the exponent n ($mn \leq 1$).

From these fits, the mean relaxation time τ or the angular frequency $\omega \approx 1/\tau$ were obtained as a function of the temperature T for each secondary and main relaxations. From these data, the activation energies E_{act} can be obtained. An Arrhenius relationship,[37] detailed in Equation 3, was considered in the case of secondary relaxations.

$$\tau(T) = \tau_0 \exp\left[\frac{-E_{act}}{RT}\right] \quad (3)$$

Where R is the ideal gas constant ($= 8.314\ J/mol{\cdot}K$). In the case of the α relaxation, a fit by the Vogel-Fulcher-Tamman relationship shown in Equation 4[38–40] was considered. This relationship, shown in Equation 4, takes into account that the main relaxations are constrained by a limit temperature T_{VFT} considered to be roughly equal to T_g-50 °C.[41]

$$\tau(T) = \tau_0 \exp\left[\frac{-E_{act}}{R\left(T - T_{VFT}\right)}\right] \quad (4)$$

Dynamic Mechanical Analyses

A TA Q800 DMA apparatus equipped with a tensile setup was utilized to characterize the thermomechanical behavior. Samples were cut to dimensions of 15x8x0.5mm^3. DMA measurements were done in a closed environment where the samples were cooled down to -150°C and then heated up to 150°C with a 3°C/min ramp rate. The frequency of the applied stress was 1 Hz, with a deformation of 0.1% and a pre-load static force of 0.01 N. The value of the main molecular α relaxation (T_α) was taken at the inflexion point on the drop of the dynamic elastic modulus E'.[12–14]

DQ ^1H Measurements

^1H Double Quanta DQ experiments were carried out on a Bruker Avance III 400 NMR equipped with a 5mm ^1H Static probe. The DQ-NMR experiments are based on Baum - Pines pulse sequences[16,17] optimized by Saalwächter.[18–23,26–29,34] Such experiments yield two components as a function of the DQ evolution time τ_{DQ} : the DQ buildup I_{DQ} and the reference decay I_{REF}. Figure SI.2 (*Support Information*) shows an example of such signals. The full magnetization of the sample I_{TOT} corresponds to the sum of I_{DQ} and I_{REF}, and comprises the response of both the dipolar coupled network and the uncoupled mobile network defects such as dangling or free (unreacted) chains. In this case, these fractions are characterized by different types of relaxation behavior. Chains fully belonging to the network relax faster and typically non-exponentially, while non-elastic chains exhibit a slower exponential relaxation.

As it has been previously described,[35] in order to properly get access to the network structure, DQ experiments must be carried out in the temperature-independent regime, *i.e.* the molecular motions probed by this technique must be effective in the fast motion regime. Preliminary studies on Neat *AE-3T* and *AE-4T* networks were carried out in this work at various temperatures and showed that this regime was reached for both networks for T_α + 140 °C (see Equation SI.1 and Figure SI.3 - *Support Information*). In this work, all of the samples were thus studied at $T = T_\alpha$ + 140 °C, ensuring that they were all tested at the same state of molecular mobility in the temperature-independent regime of the DQ signal.

In this temperature-independent regime, a DQ signal normalization has to be undertaken, allowing to discriminate the network structure influence on the DQ build-up. This normalized signal I_{nDQ} theoretically reach a plateau at the value 0.5.[32,42] The normalized signal I_{nDQ} is calculated according to Equation 5.

$$I_{nDQ} = \frac{I_{DQ}}{I_{REF} + I_{DQ} - I_{DEF}} \tag{5}$$

Equation 5 takes into account that the contribution of non-elastic chains I_{DEF} (*i.e.* dangling or free chains) has been subtracted from the total signal. A heuristic approach easily allowing the identification and subtraction of this contribution is to fit I_{DEF} through a double exponential from the $I_{REF} - I_{DQ}$ *v.s.* τ_{DQ} signal.[22,32] Extrapolating this I_{DEF} fit to $\tau_{DQ} = 0$ gives the percentage of defects (i.e. non-elastic chains) w_{DEF}. An example of this is given in Figure SI.2 (*Support Information*).

DQ NMR experiments give access to a parameter D_{res} related to an average local dynamic segmental orientation parameter. D_{res} is related to the crosslink density ν_C through Equation 6:

$$v_C \propto \frac{1}{M_C} \propto k\frac{D_{res}}{D_{stat}} \tag{6}$$

where D_{stat} is the static dipolar coupling constant and k a proportionality factor related to the details of intersegmental motions at the scale of the Kuhn length.

The numerical value of D_{res}, related to the network structure, is obtained by fitting the corresponding I_{nDQ} signal up to 0.48 by Equation 7 (See Figure SI.4 - *Support Information*).

$$I_{nDQ} = 0.5\left[1 - exp\left(-D_{res}\tau_{DQ}\right)^n\right] \tag{7}$$

where n is an exponent varying between 1 and 2. The closer n is to the value of 2, the more homogeneous the networks are.

Herein the values for k and D_{stat} were not obtained, nevertheless these factors should be identical for all samples. Hence, a quantitative comparison between all studied materials can be undertaken as described in Equation 6 by obtaining D_{res}.

Mechanical crosslink density through the Tensile modulus

To obtain an independent measurement of the crosslink density ν_C at the same temperature $T = T_\alpha + 140°\text{C}$, tensile experiments were undertaken at such temperatures for each *AE*-

3T/4T+CV samples. Measurements were carried out on an Instron 5965 universal testing machine equipped with a 100N load cell and a heating oven. The tensile testing setup was fitted inside the oven and let stabilize for one hour at each given temperature. Samples were cut with a punch so as to obtain dog bone-shaped samples of section 2x0.5 mm^2, then introduced in the oven and let to stabilize for 10 minutes before testing. The cross-head speed was set at 100 mm/min. For each sample, the Young's modulus E was determined in the elastic part of the *stress vs. strain* plot (*i.e.* up to 1% strain). From these values the mechanical crosslink density ν_{C-mech} was calculated according to Equation 8.[12,43]

$$\nu_{C-mech} = \frac{E}{\Phi RTf} \tag{8}$$

where T=T_α + 90°C, f is the network functionality (*i.e.* $f = 3$ for *AE-3T* and $f = 4$ for *AE-4T* networks), and Φ is a factor corresponding to the considered network model. Two models were considered in this work: *affine*[44] or *phantom.*[45] For the *affine* model $\Phi = 1$, while for the *phantom* model $\Phi = \frac{f-2}{f}$. Thus, for the sake of comparison, in this work the mechanical crosslink density ν_{C-mech} was calculated according to both models.

Sorption Measurements

The sorption of *CV* in neat *AE-3T/4T* networks was also characterized. Neat *AE-3T* and *AE-4T* samples of 2x2 cm^2 were immersed in sealed containers containing *CV* in excess. These containers where placed in a temperature-controlled room at 23°C. The *CV* mass intake was followed over time until the sorption equilibrium was reached, *i.e.* when no more *CV* was absorbed by the networks.[9,14,46–48] From these experiments the mass percentage intake at equilibrium of *CV* in *AE-3T/4T* networks Δm was calculated according to Equation 9.

$$\Delta m = \frac{m_{eq} - m_0}{m_0} \tag{9}$$

where m_0 and m_{eq} are respectively the network initial mass and the mass at CV sorption equilibrium.

Results and Discussion

Molecular Relaxations by Dielectric Spectroscopy

Dielectric Spectroscopy characterizations were done on *AE-3T+CV* samples in order to assess a first glance on the molecular mobility of such networks. Figure SI.5 (*Supporting Information*) shows a 3D spectrum depicting the dielectric loss permittivity ϵ'' as a function of temperature and frequency for neat *AE-3T*. Three molecular relaxations are present. These relaxations were named γ, β, and α in the order of increasing temperature appearance. At 1 Hz the relaxation temperatures for the cited relaxations were T_γ = -140°C, T_β = -85°C, and T_α = -10°C. These three relaxations were observed at similar temperatures for all *AE-3T+CV* networks.

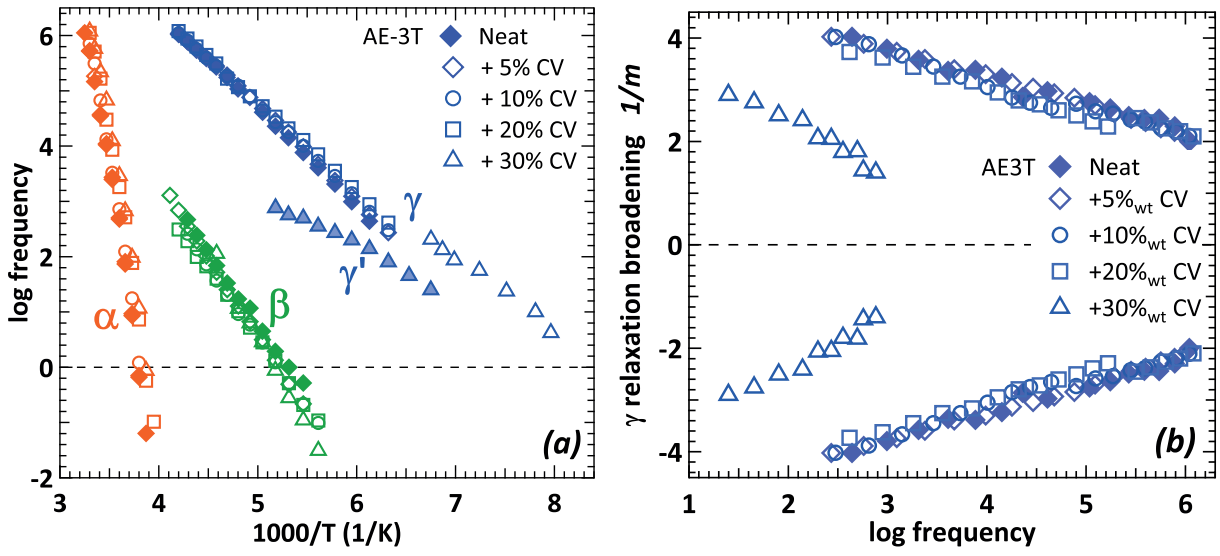

Figure 2: (a) Molecular relaxation map for the secondary (γ & β) and main (α) molecular relaxations obtained by Dielectric Spectroscopy measurements for *AE-3T+CV* samples. The γ' relaxation observed for the *AE-3T+30%$_{wt}$ CV* sample is also highlighted. (b) Broadening $1/m$ of the γ relaxation as a function of the frequency for *AE-3T+CV* samples.

The obtained activation energies E_{act} values for all relaxations are reported in Table 1.

Table 1: Calculated activation energies E_{act} for each of the observed molecular relaxations of Neat *AE-3T*.

Molecular Relaxation	E_{act} (kJ/mol)
γ	35
β	45
α	320

The calculated activation energies E_{act} for the γ and β relaxations correspond to those described in the literature for the rotation of aromatic groups (30-50 kJ/mol) and for the rotation of carbonyl functions (40-70 kJ/mol).[49] According to these values and the chemical structure of the networks, the observed relaxations can be attributed as such: the α relaxation corresponds to the main (glass) transition, and the γ and β relaxations would correspond to the rotation of the aromatic and the carbonyl groups respectively.[49] These results comfort the stated hypothesis on the nature of the secondary molecular relaxations stated above.

Moreover, Figure 2a shows the influence of *CV* on the molecular relaxations of *AE-3T*. It is globally seen that for all *CV* contents, no significant variation of the β relaxation is observed, *i.e.* the *log f v.s.* $1/T$ curves globally superpose for all *CV* contents. This is also true for the γ relaxation up to $20\%_{wt}$ *CV*. In the case of the α relaxation, a very slight shift of this relaxation towards lower temperatures is observed in the presence of *CV*, indicating that this molecule acts as a thermal plasticizer of the network. It was also found that the activation energies E_{act} for the γ, β, and α relaxations of the *AE-3T+CV* networks were fairly equal to those of the Neat material listed in Table 1.

For the *AE-3T* network containing $30\%_{wt}$ *CV* though, two different relaxations are observed: the γ relaxation common with the other networks, and a shouldering herein named γ'. This shouldering could be the signature of either two populations of aromatic rings within *AE-3T* relaxing at different temperatures or the molecular relaxation of the aromatic rings of a fraction of *CV* which would no longer be miscible in these networks.

Furthermore, Figure 2b shows the broadening of the γ relaxation for the *AE-3T* in presence of *CV* (i.e. the inverse of the Cole-Cole exponent m as defined in Equation 1). It

is clearly seen that for up to 20%$_{wt}$ *CV*, no significant impact of *CV* on the γ relaxation is observed. For *AE-3T* + 30%$_{wt}$ *CV*, the γ' relaxation is narrower. As some phase separation seems to initiate at this concentration, this would mean that the local dynamics in the domains corresponding to γ' is more homogeneous than in the materials'. –

Networks Thermomechanical Behavior

Furthermore, all *AE-3T/4T+CV* samples were characterized by DMA measurements. Figure 3 shows the elastic mechanical modulus E' obtained for all samples as a function of temperature between -150 and 70°C. As these measurements were undertaken at 1 Hz, the obtained T_α can be considered to correspond to the glass transition temperature T_g. These values are listed in Table 2. It is seen in Figure 3 and Table 2 that T_α decreases with increasing content of *CV* within the *AE-3T* and *AE-4T* networks, acting thus as a *thermal plasticizer*, as it was shown for *AE-3T* by Dielectric Spectroscopy measurements. Afterwards, a particular interest on the evolution of E' with *CV* content below T_α was paid. Thus, values of E' were taken at low temperatures, *i.e.* T_α-50°C for each sample and are listed in Table 2 as well.

For both *AE-3T* and *AE-4T* networks, it is further observed in Figure 3 and in Table 2 that E' at T_α-50°C increases when the content of *CV* increases up to 20%$_{wt}$. For 30%$_{wt}$ *CV*, E' diminishes but is still larger than that of Neat *AE-3T* and Neat *AE-4T* samples.

Moreover, tensile tests at $T = T_\alpha$+140°C were conducted on all *AE-3T* and *AE-4T* networks so as to obtain the Young's modulus E and the mechanical crosslink density ν_{C-mech} at the elastomeric regime, which are listed in Table 2. As it was experimentally challenging to obtain these values since the networks have a brittle behavior, for the sake of comparison, E' obtained by DMA at $T = T_\alpha$+50°C are also listed in Table 2. The obtained *stress vs. strain* plots are then shown in Figure 4.

These experiments show a similar phenomenon to that obtained by DMA at lower temperatures. Indeed, as it can be seen in Table 2, the Young's modulus E increases with *CV*

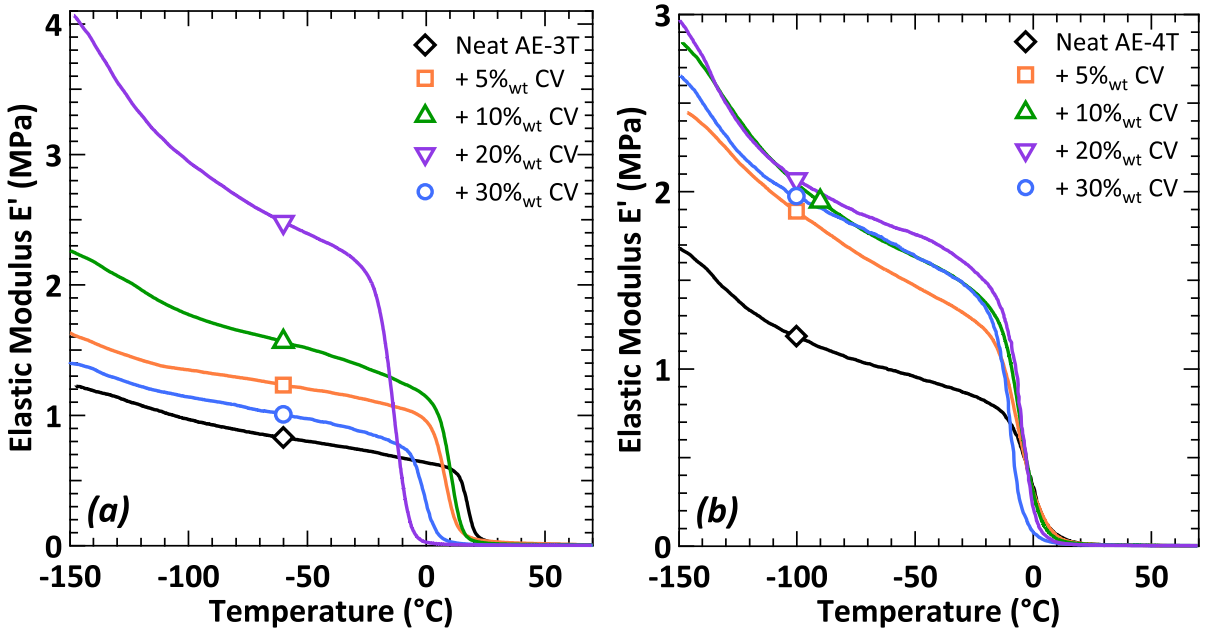

Figure 3: Elastic mechanical modulus E' obtained by DMA between -150 and 70°C for (a) *AE-3T* and (b) *AE-4T* samples for different *CV* contents.

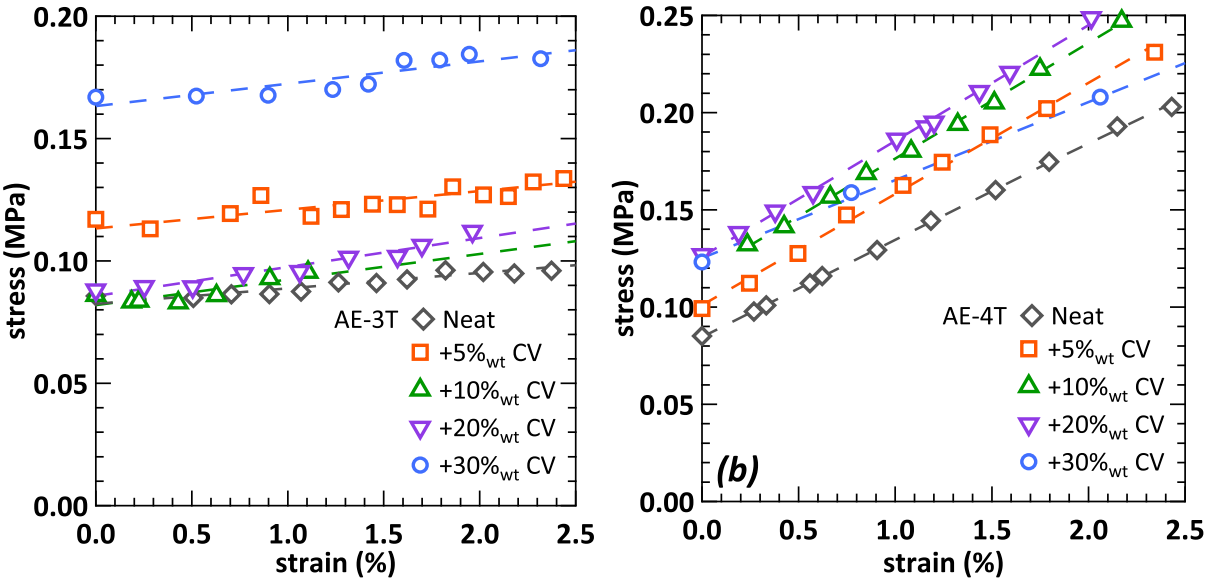

Figure 4: *Stress vs. strain* values obtained from tensile tests at $T = T_\alpha$+140°C for (a) *AE-3T* and (b) *AE-4T* samples for different *CV* contents. The dashed lines are linear fits from which the Young's Moduli E were calculated.

Table 2: DMA, Tensile testing and DQ ^1H NMR results obtained for the studied *AE-3T* and *AE-4T* networks containing various amounts of *CV*.

Network			DMA		Tensile testing			DQ ^1H NMR		
		T_α (°C)	E' @ T_α-50°C (GPa)	E' @ T_α+50°C (MPa)	E @ T_α+140°C (MPa)	ν_{C-mech} affine $\times 10^4$ (mol/g)	ν_{C-mech} phantom $\times 10^4$ (mol/g)	$D_{res}/2\pi$ (Hz)	w_{def} (%)	n
AE-3T	Neat	16	0.75	6.33	0.63	0.59	1.77	149.5	13.4	1.19
	+5%$_{wt}$ *CV*	8	1.18	11.59	0.76	0.72	2.17	172.2	15.7	1.23
	+10%$_{wt}$ *CV*	10	1.46	7.52	1.05	0.99	2.98	211.4	9.3	1.30
	+20%$_{wt}$ *CV*	-14	2.51	4.22	1.18	1.18	3.56	233.4	11.4	1.03
	+30%$_{wt}$ *CV*	1	0.97	3.19	0.91	0.88	2.54	176.1	15.2	1.09
AE-4T	Neat	-2	0.95	4.37	5.00	3.66	7.31	425.3	2.5	1.24
	+5%$_{wt}$ *CV*	-5	1.50	5.56	5.71	4.21	8.41	481.1	2.1	1.29
	+10%$_{wt}$ *CV*	-6	1.67	5.69	5.95	4.39	8.78	512.0	2.1	1.28
	+20%$_{wt}$ *CV*	-6	1.79	4.82	5.95	4.40	8.79	514.4	1.5	1.32
	+30%$_{wt}$ *CV*	-10	1.71	4.00	4.00	2.98	5.97	478.4	2.9	1.29

content up to 20%$_{wt}$ for both *AE-3T* and *AE-4T* networks. Again, for networks containing 30%$_{wt}$ *CV*, E diminishes. Consequently, the apparent mechanical crosslink density ν_{C-mech}, also listed in Table 2 (calculated by both the affine and phantom models) follows the same trend as E, that is ν_{C-mech} increases with *CV* content up to 20%$_{wt}$.

It is firstly seen that the experimental ν_{C-mech} values for both *AE-3T/4T* networks are lower than the theoretical stoichiometric ones. For *AE-3T* the experimental values differ by almost an order of magnitude (ie. 1.56×10^{-3} mol/g) whereas for *AE-4T*, the measured ν_{C-mech} are relatively closer to the theoretical estimation (i.e. 1.17×10^{-3} mol/g). Moreover, and more surprisingly, the experimental ν_{C-mech} values for *AE-4T* networks are greater than those for *AE-3T*. This is an unexpected result as in theory the *AE-3T* network should be denser and it ws shown that all SH functions have completely reacted. Furthermore, the presence of *CV* in the networks does not modify the experimental ν_{C-mech} values. This phenomenon will be further discussed and detailed.

In this given case, regardless of the *AE-3T/4T* networks morphology, *CV* can be then considered to act as a *mechanical antiplastizicer* of the networks. This result is also counter-intuitive as it would be expected that this molecule would have a mechanical plasticizer effect since its presence leads to a drop of T_α. A hypothesis to explain the rise of E' and E in presence of *CV* would be that this molecule may eventually strongly interact physically with the *AE-3T/4T* network, which will be further addressed.

Network structures as characterized by ^1H *DQ* NMR

Neat *AE-3T* and *AE-4T* networks were characterized by ^1H *DQ* analyses. Figure SI.6a (*Support Information*) presents the I_{nDQ} signal obtained by normalizing the *DQ* build-up measured at $T = T_\alpha$+140 °C by Equation 5 for these networks as a function of τ_{DQ}. It is clearly seen in Figure SI.6a (*Support Information*) that the *AE-4T* network possesses a steeper I_{nDQ} signal than that of *AE-3T*. This means that the *AE-4T* network has a larger dipolar residual constant D_{res}, which can be interpreted as a larger crosslink density ν_C (*i.e.*

Equation 6) than that of *AE-3T* network. This observation does not follow the expected theoretical behavior detailed above, but is in perfect accordance to the results obtained by tensile testing at $T = T_\alpha$+140 °C in which the mechanical crosslink-density ν_{C-mech} is also larger for the *AE-4T* network. Then, the I_{nDQ} signals for both neat networks were fitted by Equation 7 so as to obtain the numerical values of D_{res}. These values are listed in Table 2. The I_{nDQ} signals for both networks are plotted in Figure SI.6b (*Support Information*) as a function of the normalized DQ time $D_{res}\tau_{DQ}$.

This plot shows that the *AE-3T* and *AE-4T* networks I_{nDQ} signals superpose fairly well with each other. This indicates that these two materials possess a similar network morphology apart from different crosslink densities. This seems logical since the chemical structure of the monomers is the same, the only parameter that changes is the functionality of the thiol crosslinker. Moreover, from the I_{nDQ} normalization from Equation 5, the percentage of defects w_{DEF} (*i.e.* physically-entangled and free chains) was obtained. These values are also presented in Table 2. The w_{DEF} obtained values are for *AE-4T* show that this material has *ca.* 6 times less defects than *AE-3T* networks. Thus, these two results show that *AE-4T* inherently has a higher crosslink density and a more organized network structure than that of *AE-3T* networks.

Afterwards, the influence of the presence of CV in the *AE-3T* and *AE-4T* networks was assessed. Firstly, regarding the percentage of defects, it is seen that the presence of CV in both networks does not induce a large variation of w_{DEF}. This is quite unexpected since if CV molecules would behave as a solvent freely diffusing within the network, they would contribute to the non-elastic part of the material, i.e. to the so-called *defect* part of the signal. Conversely, they seem to contribute to the *elastic DQ* signal. This would mean that they are strongly coupled to network chains, in such a way that their local dynamics is anisotropic, reflecting that of elastic chains. This important observation will be further discussed in the next section.

Then, the I_{nDQ} signals are plotted in Figures 5a and 5b as a function of τ_{DQ} obtained

at $T = T_\alpha$+140 °C and normalized according to Equation 5 respectively for the *AE-3T* and *AE-4T* networks containing various percentages of *CV*.

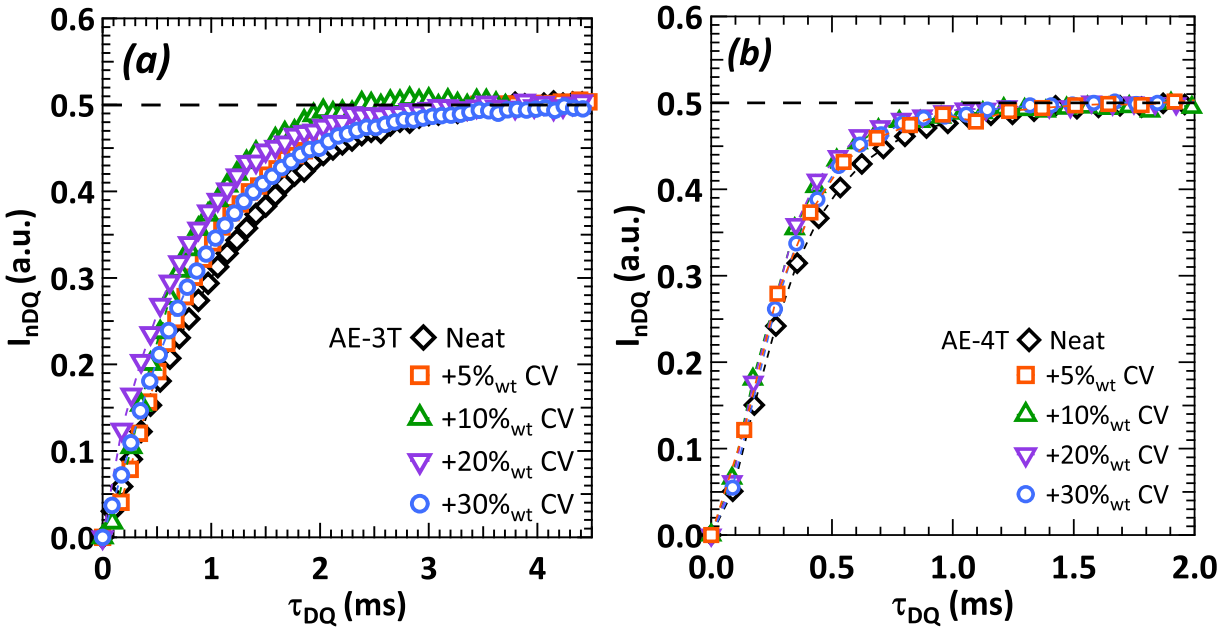

Figure 5: I_{nDQ} signals as a function of τ_{DQ} obtained by ^1H *DQ*-NMR for the (a) *AE-3T* and (b) *AE-4T* at $T + T_\alpha$+140 °C containing various percentages of *CV*.

It is seen in Figures 5a and 5b that the presence of *CV* has a clear influence on the I_{nDQ} signals of *AE-3T* and *AE-4T* networks. This is better seen in Figures SI.7a and SI.7b (*Support Information*) which correspond to zoom-ins of the I_{nDQ} signals. All of these plots show that for both *AE-3T* and *AE-4T* networks, when the amount of *CV* increases, the I_{nDQ} signal becomes steeper. This phenomena is observed for *CV* amounts between $0\%_{wt}$ and $20\%_{wt}$. For samples containing $30\%_{wt}$ *CV* though, the I_{nDQ} slope becomes less steep when compared to the networks containing $20\%_{wt}$ *CV*. To deepen this analysis, the I_{nDQ} signals were fitted according to Equation 7 to obtain the numerical value of the residual dipolar constant D_{res} for each network as it was done for the neat networks before. The obtained D_{res} values are listed in Table 2.

It is observed that the values of D_{res} *increase with CV* content up to $20\%_{wt}$, and then they drop for 30 $\%_{wt}$ *CV* content, exhibiting a similar behavior as obtained for E' and E. To further understand these observations, I_{nDQ} was plotted as a function of the reduced *DQ*

time $D_{res}\tau_{DQ}$ and are shown in Figure 6.

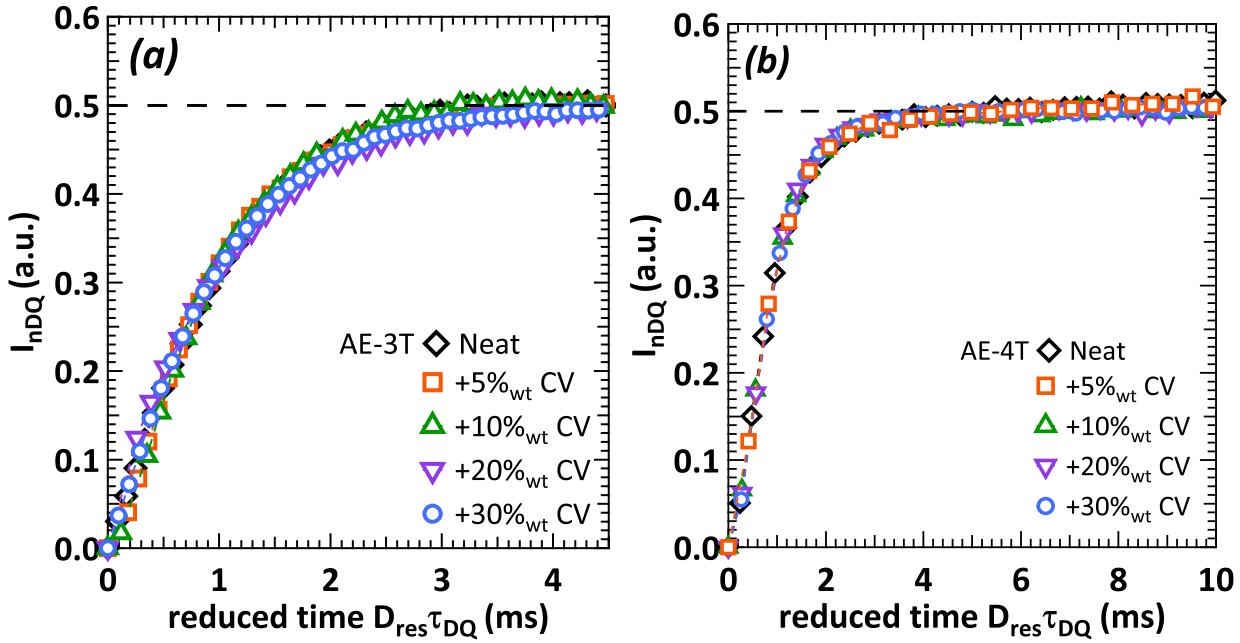

Figure 6: I_{nDQ} signals as a function of the normalized DQ time $D_{res}\tau_{DQ}$ obtained by ^1H DQ-NMR for the (a) *AE-3T* and (b) *AE-4T* at $T + T_\alpha$+140 °C containing various percentages of *CV*.

As it was the case for the neat *AE-3T* and *AE-4T* networks, it is seen in Figure 6 that for such materials containing *CV* the curves superpose fairly well with each other, specially in the case of *AE-4T* networks. This would mean that all samples have a similar network morphology. As *CV* does not hinder or interfere on the chemical reaction between *AE* and *3T* or *4T*,[6–8] the difference of the D_{res} values (*i.e.* or ν_C, or the I_{nDQ} slope) between networks would be certainly and solely due to the physical presence of *CV*.

Carvacrol sorption at equilibrium in Neat Networks

Table 3 lists the Δm values obtained for the sorption of *CV* in *AE-3T* and *AE-4T* neat networks. It can be seen that the maximum percentage of *CV* introduced in this work in the *AE-3T/4T* reactive media, *i.e.* 30%$_{wt}$, is lower than the maximum amount of *CV* absorbed by neat *AE-3T/4T* networks, albeit for *AE-4T* whose Δm equilibrium value is close to 30%$_{wt}$. Moreover, it is also observed that *AE-3T* is capable of absorbing *ca.* 7 times more

CV than *AE-4T*. As it has been thoroughly characterized, the measured crosslink density ν_C of *AE-4T* is larger than that of *AE-3T* networks. More free volume is then available in these latter materials, facilitating thus the sorption of *CV*.

Table 3: Mass percentage at sorption equilibrium Δm for Neat *AE-3T* and *AE-4T* networks immersed in *CV*.

	Δm (%)
AE-3T + CV	245
AE-4T + CV	34

Multiscale Analysis

In order to better understand and assess the effect of *CV* on *AE-3T/4T* networks, a multi-scale approach was undertaken. To do so, the D_{res} values (*i.e.* ^1H *DQ*-NMR) are plotted in Figure 7 as a function of the mechanical crosslink density ν_{C-mech} calculated from the *phantom* model (*i.e.* tensile testing). Figure SI.8 (*Support Information*) presents the same plot with ν_{C-mech} calculated from the *affine* model.

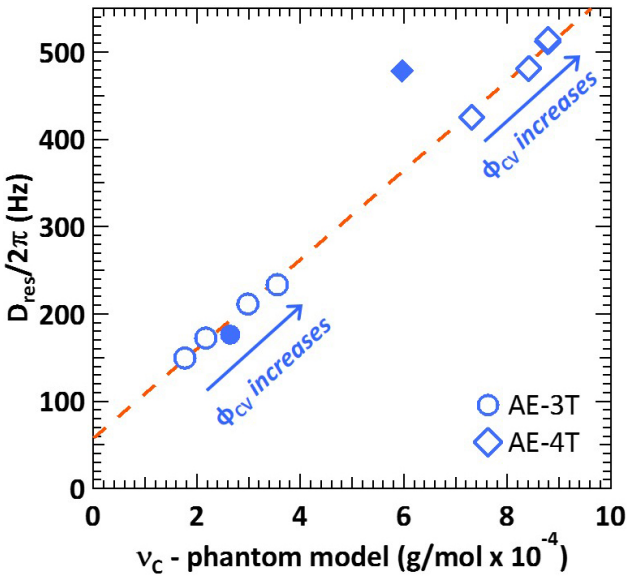

Figure 7: D_{res} obtained by ^1H *DQ*-NMR for the *AE-3T+CV* and *AE-4T+CV* samples as a function of the ν_C calculated from the *phantom* model. The full markers correspond to the samples containing $30\%_{wt}$ *CV*. The dashed line is a linear fit and is a guide for the eyes.

Figure 7 shows that there is a *same* linear relationship between D_{res} and ν_{C-mech} for both the *AE-3T* and *AE-4T* networks containing up to 20%$_{wt}$ *CV*. The values for networks containing 30%$_{wt}$ *CV* (*i.e.* full markers) do not follow this linear trend, especially that for *AE-4T*. Furthermore, when comparing Figure SI.8 (*Support Information*) with Figure 7 it seen that the network model that better fits this relationship is the *phantom model*. Indeed, apart from the points corresponding to 30%$_{wt}$ *CV*, all values follow perfectly the linear trend. Such a perfect linear correlation between D_{res} and the mechanical modulus has been already observed as well in elastomers.[32,5] Moreover, it was also proposed long ago by Cohen-Addad.[51]

It could be thought that the increase of ν_{C-mech} in presence of *CV* might due to the network hardening induced by this molecule. In the case of Neat *AE-3T/4T* networks in contact with CV after the network crosslinking, two competing effects may take place: an increase of local mobility leading to a decrease of D_{res},[52,53] or an increase of local chain stretching due to swelling, leading to an increase of D_{res}.[54] As in our materials the network is quite tight, with significantly higher crosslink densities than in usual elastomers and gels, it may be thought that this second effect might be predominant. This would explain the increase of ν_{mecha} for Neat *AE-3T/4T* networks in the presence of *CV* after the network reticulation.[54–57] However, in this work *CV was added to the reactant media*, which in turn was well-homogenized *before the photo-chemical reticulation* of *AE* with *3T* or *4T*. As already mentioned, *CV* is chemically inert in this reaction[6–8] and its size is significantly smaller than that of a *AE-3T/4T* monomer. Indeed *CV* molecular weight is M_{CV}=150 g/mol whereas the molecular weight between crosslinks for *AE-3T/4T* is of M_C=426 g/mol. Moreover it does not influence the percentage of defects w_{DEF} of these networks. Therefore it would be easily enclosed in the networks free volume *without inducing local stretching of polymer chains*. The observed effect would then be due essentially to physical interactions of *CV* with the network chains inducing hardening of the network.

Furthermore, one important outcome of this work is that the elastic response seems to be

decorrelated from the crosslink density for the *AE-3T* network. This may be related to the notion of rigidity percolation.[58] For a network made of elastic strands connected together with a connectivity f, there is a threshold f_c below which the network becomes floppy, i.e. the elastic modulus vanishes (while it is still topologically connected) as described in Figure 8a[59] (*and references cited therein*). Far enough above this threshold, the elastic modulus is given by Equation 8.

f_c has been estimated for some ordered lattices.[60–65] A realistic value for f_c could be around 3 or slightly below 3, which may explain the unexpectedly low modulus of the *AE- 3T* network. However, further work would be needed to assess this hypothesis.

It is interesting to observe that, besides the macroscopic elastic behavior as measured by the elastic modulus, the average local chain elasticity as measured by NMR is also much lower for *AE-3T* and is nicely correlated to the macroscopic behavior, as illustrated in Figure 7. Another, slightly different but related, way of analyzing the results would be to consider that the *AE-3T* monomer is prone to form aggregates not connected to the percolating elastic network, as illustrated in Figure 8b, and that this tendency is more pronounced for *3T* than for *4T*, in relation to the lower connectivity of *3T*. This would qualitatively be coherent with both the lower modulus E and the higher fraction of *defects* w_{def} measured by ^1H *DQ* NMR.

Finally, all of the presented results obtained by combining the utilized experimental techniques highlight the following assertions:

- First, the *AE-3T/4T* networks experimental crosslink density is smaller than that calculated for an ideal case, especially for *AE-3T*. This could be explained either by the reaching of the percolation limit in which the elastic modulus in a network would disappear or by the formation of nanoaggregates within the materials. When comparing both networks, the *AE-4T* crosslink network density ν_{C-mech} is four times larger and not 4/3 smaller than that of *AE-3T*. Experimentally, this can be explained by the difference on the percentage of *defects* w_{def} of both networks: *AE-4T* has ca. 2.5%

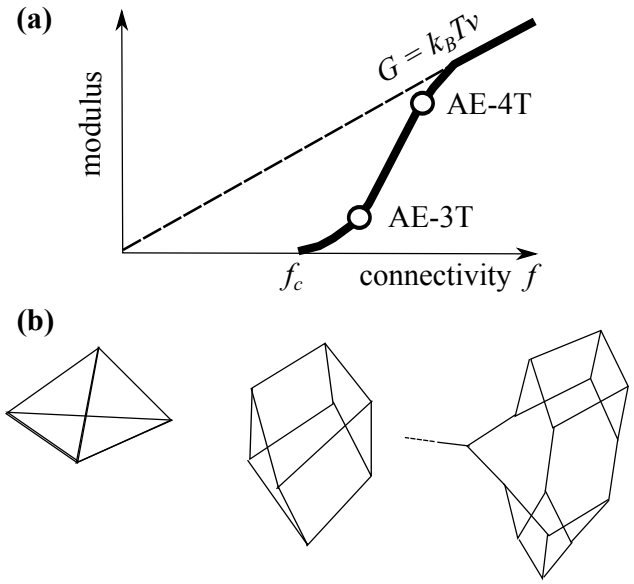

Figure 8: (a) Rigidity percolation, below f_c the elastic modulus vanishes and (b) Schematics illustrating the possibility of forming unconnected or dangling nanoaggregates within a network of connectivity $f = 3$.

defects while for *AE-4T* this percentage increases to ca. 14%. This explains the vast difference of *experimental* E at $T = T_\alpha$+140 °C, and D_{res} between networks.

- Second, the presence of CV induces an increase of E', E, D_{res} and ν_{C-mech} up to 20%$_{wt}$ CV. This means that CV induces a rise of local chain stretching, which could as well be expressed in terms of an increase on *apparent crosslink density* within the *AE-3T/4T* networks.

- Third, all samples follow a *single* linear trend for D_{res} *v.s.* ν_{C-mech}. This would mean that as long as the overall network chemical structure does not vary (with the only variable being the functionality of the cross-linker) a direct relationship between the network structure, the cross-link density, and thus the macroscopic mechanical properties can be established.

- Fourth, E', E, D_{res} and ν_{C-mech} values drop for networks containing 30%$_{wt}$ CV. Coupled with the presence of a γ' relaxation observed for this content in *AE-3T* networks, these results show that CV has a limited miscibility within *AE-3T/4T* and that it has

been reached for 30%$_{wt}$. In this case two different populations of *CV* would co-exist in the networks. One population that would interact directly with the polymer chains, and another one that would be free within the material perhaps within solvent-rich domains.

As such, all of the results presented in this paper confirm that *CV* undoubtedly interacts with the *AE-3T/4T* networks through intermolecular physical bonds. As both *CV* and the networks possess aromatic functions, the presence of π-π bonds is fairly probable. Such bonds, which are schematically represented in Figure 9, have a relative high bonding energy of *ca.* 10 to 25 kJ/mol.[66,67] The presence of such bonds would might then yield a rise on the crosslink density of the material as such bonds would act as physical cross-links, inducing a rise on the thermomechanical moduli as well as on the measured crosslink densities.

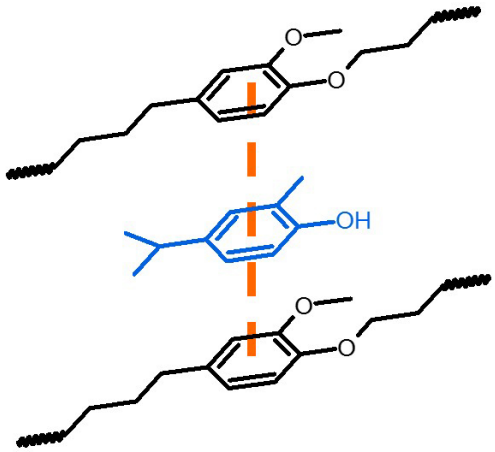

Figure 9: Proposed π-π interactions resulting in physical crosslinks between the aromatic rings of *CV* (middle) and *AE-3T/4T* networks.

Conclusion

This work has dealt with establishing the relationship between the inner structure, the molecular mobility, and the thermomechanical behavior of biosourced eugenol-based antibacterial networks containing various concentrations of carvacrol. Through a robust thermodynamic

and experimental approach combining Dielectric Spectroscopy, DMA, Tensile testing, and $DQ\ ^1H$ Time domain NMR, it was shown that the presence of carvacrol linearly influences the thermomechanical behavior of diallyl-eugenol networks. Indeed, it was observed by Dielectric Spectroscopy that carvacrol had an influence on the γ relaxation of these networks, which corresponds to the motions of aromatic rings. Furthermore, DMA showed that although carvacrol up to $20\%_{wt}$ acts as a thermal plasticizer, *i.e.* it diminishes T_α, it induces a rise of the elastic E' and Young's E moduli. Finally, by combining Tensile testing and $DQ\ ^1H$ Time Domain NMR, it was shown that the crosslink density ν_C of the diallyl-eugenol based networks increased with carvacrol content up to $20\%_{wt}$. Since carvacrol does not react with nor swells the diallyl-eugenol networks, the increase in crosslink density is due to the presence of physical crosslink nodes. These nodes are induced by strong $\pi - \pi$ intermolecular physical interactions between the aromatic rings of carvacrol and diallyl-eugenol. For carvacrol contents over $20\%_{wt}$, it was shown that E', E, and ν_C diminished, meaning that this molecule had reached its miscibility limit. To sum up, the strategy proposed in this work permits a better understanding of these novel antibacterial networks as regards the influence of the materials structure on its functional properties. Moreover, this study can be promptly extended to similar biobased networks and as such it will be expanded for analogous networks containing diverse additives enhancing their inherent behavior.

Funding

This project was kindly funded by both the *Institut de Chimie et des Matériaux Est* and the *Faculté des Sciences et Technologie - UPEC* through a *Jeunes Chercheurs* project.

Acknowledgement

The authors are deeply grateful towards Alvaro Quinteros-Sedano, Nora Hamel, Béatrice Huynh, Amel Sakhi, and Marion Brosset for the DMA and tensile test characterizations,

and towards Cédric Lorthoir for sharing the ^1H *DQ* NMR pulse program sequence used in this study.

References

(1) DuPrez, F.; Raquez, J.-M.; Dubois, P. Biobased Polymers and Related Materials. *European Polymer Journal* **2013**, *49*, 753–996.

(2) Babu, R. P.; O'Connor, K.; Seeram, R. Current progress on bio-based polymers and their future trends. *Prog. Biomater.* **2013**, *2*, 8–24.

(3) Rebouillat, S.; Pla, F. Recent Strategies for the Development of Biosourced-Monomers, Oligomers and Polymers-Based Materials: A Review with an Innovation and a Bigger Data Focus. *Journal of Biomaterials and Nanobiotechnology* **2016**, *7*, 167–213.

(4) Froidevaux, V.; Negrell, C.; Caillol, S.; Pascault, J.-P.; Boutevin, B. Biobased Amines: From Synthesis to Polymers; Present and Future. *Chem. Rev.* **2016**, *116*, 14181–14224.

(5) Modjinou, T.; Versace, D.-L.; Abbad-Andallousi, S.; Bousserrhine, N.; Babinot, J.; Langlois, V.; Renard, E. Antibacterial Networks Based on Isosorbide and Linalool by Photoinitiated Process. *ACS Sustainable Chem. Eng.* **2015**, *3*, 1094–1100, DOI: 10.1021/acssuschemeng.5b00018.

(6) Modjinou, T.; Rodriguez-Tobias, H.; Morales, G.; Versace, D.-L.; Langlois, V.; Grande, D.; Renard, E. UV-cured thiol–ene eugenol/ZnO composite materials with antibacterial properties. *RCS Advances* **2016**, *6*, 88135–88142, DOI: 10.1039/C6RA18551G.

(7) Modjinou, T.; Versace, D.-L.; Abbad-Andallousi, S.; Bousserrhine, N.; Dubot, P.; Langlois, V.; Renard, E. Antibacterial and antioxidant bio-based networks derived from

eugenol using photo-activated thiol-ene reaction. *React. Funct. Polym.* **2016**, *101*, 47–53, DOI: 10.1016/j.reactfunctpolym.2016.02.002.

(8) Glaive, A.; Modjinou, T.; Versace, D.-L.; Abbad-Andallousi, S.; Dubot, P.; Langlois, V.; Renard, E. Design of Antibacterial and Sustainable Antioxidant Networks Based on Plant Phenolic Derivatives Used As Delivery System of Carvacrol or Tannic Acid. *ACS Sustainable Chem. Eng.* **2017**, *5*, 2320–2329, DOI: 10.1021/acssuschemeng.6b02655.

(9) de Anda, A. R.; Fillot, L.-A.; Rossi, S.; Long, D.; Sotta, P. Influence of the sorption of polar and non-polar solvents on the glass transition temperature of polyamide 6,6 amorphous phase. *Polym. Eng. Sci.* **2011**, *51*, 2129–2135, DOI: 10.1002/pen.22064.

(10) McCrumm, N. G., Read, B. E., Williams, G., Eds. *Anelastic and Dielectric Effects on Polymer Solids*; Dover: New York, 1991.

(11) Kremer, F., Schoenhalls, A., Eds. *Broadband Dielectric Spectroscopy*; Springer: Berlin, 2003.

(12) Hallary, J.-L., Lauprêtre, F., Monnerie, L., Eds. *Polymer Materials, Macroscopic Properties and Molecular Interpetrations*; John Wiley & Sons: Hoboken, 2010.

(13) Ceausescu, E., Ed. *Research Work on Synthesis and Characterization of Macromolecular Compounds*; Editura Academiei: Bucharest, 1974.

(14) de Anda, A. R.; Fillot, L.-A.; Long, D.; Sotta, P. Influence of the amorphous phase molecular mobility on impact and tensile properties of polyamide 6,6. *J. Appl. Polym. Sci.* **2016**, *133*, 43457, DOI: 10.1002/app.43457.

(15) Yen, Y.-S.; Pines, A. Multiple-quantum NMR in solids. *J. Chem. Phys. Part II* **1983**, *78*, 3579–3582.

(16) Baum, J.; Munowitz, M.; Garroway, A. N.; Pines, A. Multiplequantum dynamics in solid state NMR. *J. Chem. Phys.* **1985**, *83*, 2015–2025, DOI: 10.1063/1.449344.

(17) Baum, J.; Pines, A. NMR Studies of Clustering in Solids. *J. Am. Chem. Soc.* **1986**, *108*, 7447–7454.

(18) Saalwächter, K.; Ziegler, P.; Spyckerelle, O.; Haidar, B.; Vidal, A.; Sommer, J. U. ^1H multiple-quantum nuclear magnetic resonance investigations of molecular order distributions in poly(dimethylsiloxane) networks: Evidence for a linear mixing law in bimodal systems. *J. Chem. Phys.* **2003**, *119*, 3468–3482.

(19) Saalwächter, K. ^1H multiple-quantum nuclear magnetic resonance investigations of molecular order in polymer networks. II. Intensity decay and restricted slow dynamics. *J. Chem. Phys.* **2004**, *120*, 454–464, DOI: 10.1063/1.1630561.

(20) Saalwächter, K.; Kleinschmidt, F.; Sommer, J.-U. Swelling Heterogeneities in End-Linked Model Networks: A Combined Proton Multiple-Quantum NMR and Computer Simulation Study. *Macromolecules* **2004**, *37*, 8556–8568, DOI: 10.1021/ma048803k.

(21) Saalwächter, K.; Herrero, B.; López-Manchado, M. A. Chain Order and Cross-Link Density of Elastomers As Investigated by Proton Multiple-Quantum NMR. *Macromolecules* **2005**, *38*, 9650–9660, DOI: 10.1021/ma051238g.

(22) Saalwächter, K. Proton multiple-quantum NMR for the study of chain dynamics and structural constraints in polymeric soft materials. *Prog. Nucl. Magn. Reson. Spectrosc.* **2007**, *51*, 1–35.

(23) Chassé, W.; Schlögl, S.; Riess, G.; Saalwächter, K. Inhomogeneities and local chain stretching in partially swollen networks. *Soft Matter* **2013**, *9*, 6943–6954, DOI: 10.1039/c3sm50195g.

(24) Valentín, J.; Mora-Barrantes, I.; Carretero-González, J.; López-Manchado, M.; Sotta, P.; Long, D.; Saalwächter, K. Novel experimental approach to evaluate filler-elastomer interactions. *Macromolecules* **2010**, *43*, 334–346, DOI: 10.1021/ma901999j.

(25) Mansilla, M.; Valentín, J.; López-Manchado, M.; González-Jiménez, A.; Marzocca, A. Effect of entanglements in the microstructure of cured NR/SBR blends prepared by solution and mixing in a two-roll mill. *E. Polym. J.* **2016**, *81*, 365–375, DOI: 10.1016/j.eurpolymj.2016.06.023.

(26) Lorthioir, C.; Randriamahefa, S.; Deloche, B. Some aspects of the orientational order distribution of flexible chains in a diblock mesophase. *J. Chem. Phys.* **2013**, *139*, 224903, DOI: 10.1063/1.4838375.

(27) Lorthioir, C.; Deloche, B. Heterogeneous behavior of free chain-ends in a lamellar diblock copolymer: segmental dynamics and ordering, as probed by ^2H solid-state NMR. *Colloid Polym. Sci.* **2014**, *292*, 1841–1851.

(28) Saalwächter, K.; Heuer, A. Chain Dynamics in Elastomers As Investigated by Proton Multiple-Quantum NMR. *Macromolecules* **2006**, *39*, 3291–3301, DOI: 10.1021/ma052567b.

(29) Chávez, F. V.; Saalwächter, K. Time-Domain NMR Observation of Entangled Polymer Dynamics: Analytical Theory of Signal Functions. *Macromolecules* **2011**, *44*, 1560–1569, DOI: 10.1021/ma102571u.

(30) Martin-Gallego, M.; González-Jiménez, A.; Verdejo, R.; López-Manchado, M. A.; Valentín, J. L. Epoxy Resin Curing Reaction Studied by Proton Multiple-Quantum NMR. *J. Polym. Sci. Part B Polym. Phys.* **2015**, *53*, 1324–1332, DOI: 10.1002/polb.23767.

(31) Gjersing, E.; Chinn, S.; Giuliani, J. R.; Herberg, J.; Maxwell, R. S.; Eastwood, E.; Bowen, D.; Stephens, T. Investigation of Network Heterogeneities in Filled, Trimodal, Highly Functional PDMS Networks by ^1H Multiple Quantum NMR. *Macromolecules* **2007**, *40*, 4953–4962, DOI: 10.1021/ma0620924.

(32) Vieyres, A.; Pérez-Aparicio, R.; Albouy, P.-A.; Sanseau, O.; Saalwächter, K.; Long, D. R.; Sotta, P. Sulfur-Cured Natural Rubber Elastomer Networks: Correlat-

ing Cross-Link Density, Chain Orientation, and Mechanical Response by Combined Techniques. *Macromolecules* **2013**, *43*, 889–899, DOI: 10.1021/ma302563z.

(33) Giuliani, J. R.; Gjersing, E. L.; Chinn, S. C.; Jones, T. V.; Wilson, T. S.; Alviso, C. T.; Herberg, J. L.; Pearson, M. A.; Maxwell, R. S. Thermal Degradation in a Trimodal Poly(dimethylsiloxane) Network Studied by 1H Multiple Quantum NMR. *J. Phys. Chem. B* **2007**, *111*, 12977–12984, DOI: 10.1021/jp075840f.

(34) Gabrielle, B.; Lorthioir, C.; Lauprêtre, F. Thermal Aging of Interfacial Polymer Chains in Ethylene-Propylene-Diene Terpolymer/Aluminum Hydroxide Composites: Solid-State NMR Study. *J. Phys. Chem. B* **2011**, *115*, 12392–12400, DOI: 10.1021/jp207084j.

(35) van Bochove, B.; Spoljaric, S.; Seppälä, J.; Sotta, P.; de Anda, A. R. Multiscale characterization of biocompatible Poly(trimethylene carbonate) photoreticulated networks by coupling of DMA and Multiple Quanta ^1H Solid State NMR measurements. *ACS Applied Polymer Materials* **2019**, *1*, 1811–1820, DOI: 10.1021/acsapm.9b00338.

(36) Havriliak, S.; Negami, S. A complex plane representation of dielectric and mechanical relaxation processes in some polymers. *Polymer* **1967**, *8*, 161–210.

(37) Laidler, K. J. A Glosary of Therms Used in Chemical Kinetics, Including Reaction Dynamics. *Pure & Appl. Chem.* **1996**, *68*, 149–192.

(38) Vogel, H. Das temperatur abhaengigkeit gesetz der viskositaet von fluessigkeiten. *Phys. Z.* **1921**, *22*, 645–646.

(39) Fulcher, G. S. Analysis of recent measurements of the viscosity of glasses. *Ceram. Soc.* **1925**, *8*, 339–355.

(40) Tammann, G.; Hesse, W. Die abhaengigkeit der viskositaet von der temperatur bei unterkuehlten fluessigkeiten. *Z. Anorg. Allg. Chem.* **1926**, *156*, 245–257.

(41) Williams, M. L.; Landel, R. F.; Ferry, J. D. The temperature dependence of relaxation mechanisms in amorphous polymers and other glass-forming liquids. *J. Am. Chem. Soc.* **1955**, *77*, 3701–3707.

(42) Pérez-Aparicio, R.; Vieyres, A.; Albouy, P.-A.; Sanseau, O.; Vanel, L.; Long, D. R.; Sotta, P. Reinforcement in Natural Rubber Elastomer Nanocomposites: Breakdown of Entropic Elasticity. *Macromolecules* **2013**, *46*, 8964–8972, DOI: 10.1021/ma401910c.

(43) Landau, L. D., Lifshitz, E. M., Eds. *Theory of Elasticity*; Pergamon Press: Oxford, 1970.

(44) Flory, P. J., Ed. *Principles of Polymer Chemistry*; Cornell University Press: Ithaca, 1953.

(45) James, H. M.; Guth, E. Statistical Thermodynamics of Rubber Elasticity. *J. Chem. Phys.* **1953**, *21*, 1039–1049, DOI: 10.1063/1.1699106.

(46) Crank, J., Ed. *The Mathematics of Diffusion*; Oxford University Press: London, 1970.

(47) Landau, L. D., Lifshitz, E. M., Eds. *Statistical Physics Vol. V Theoretical Physics*; Mir Editions: Moscow, 1967.

(48) de Anda, A. R.; Fillot, L.-A.; Preda, F.; Rossi, S.; Long, D.; Sotta, P. Sorption and plasticization effects of ethanol–toluene–isooctane ternary mixtures in polyamide 6,6 and induced plasticization effects. *Eur. Polym. J.* **2014**, *55*, 199–209, DOI: 10.1002/app.43457.

(49) Haward, R. N., Young, R. J., Eds. *The Physics of Glassy Polymers*; Springer: Dordrecht, 1997.

(50) Valentín, J.; Carretero-González, J.; Mora-Barrantes, I.; Chassé, W.; Saalwächter, K. Uncertainties in the Determination of Cross-Link Density by Equilibrium Swelling

Experiments in Natural Rubber. *Macromolecules* **2008**, *41*, 4717–4729, DOI: 10.1021/ma8005087.

(51) Cohen-Addad, J. P. NMR and Gel Elasticity Interrelationship. *Macromolecules* **1989**, *22*, 147–151, DOI: 10.1021/ma00191a028.

(52) Sotta, P.; B.Deloche,; J.Herz, Effect of dilution on the orientational order induced in strained polymer networks, as measured by ^2H nuclear magnetic resonance. *Polymer* **1988**, *29*, 1171–1178, DOI: 10.1016/0032-3861(88)90041-9.

(53) Cohen-Addad, J. P.; Faure, J. Free volume and chain constraints in cis-1,4-polybutadiene as observed by high resolution NMR linewidth. *J. Chem. Phys.* **1974**, *61*, 1571, DOI: 10.1063/1.1682102.

(54) Cohen-Addad, J. P.; Domard, M.; Herz, J. NMR observation of the swelling process of polydimethylsiloxane networks. Average orientational order of monomeric units. *J. Chem. Phys.* **1982**, *76*, 2744, DOI: 10.1063/1.443260.

(55) Croll, S. Residual Strain Due to Solvent Loss From a Crosslinked Coating. *Journal of Coatings Technology* **1981**, *53*, 85–92.

(56) Myung, D.; Koh, W.; Ko, J.; Hu, Y.; Carrasco, M.; Noolandi, J.; Ta, C. N.; Frank, C. W. Biomimetic strain hardening in interpenetrating polymer network hydrogels. *Polymer* **2007**, *48*, 5376–5387, DOI: 10.1016/j.polymer.2007.06.070.

(57) Liang, S.; Yu, Q. M.; Yin, H.; Wu, Z. L.; Kurokawa, T.; Gong, J. P. Ultrathin tough double network hydrogels showing adjustable muscle-like isometric force generation triggered by solvent. *Chemical Communications* **2009**, *48*, 7518–7520, DOI: 10.1039/B916581A.

(58) Thorpe, M. In *Rigidy percolation, in: Physics of Disordered Materials*; Adler, D., Ed.; Plenum Press: New York, 1985; pp 55–61.

(59) Long, D.; Sotta, P. In *Numerical Simulation for the Mesoscale Deformation of Disordered Reinforced Elastomers in Modeling of Soft Matter*; Calderer, M.-C. T., Terentjev, E. M., Eds.; Springer: New York, 2005; pp 205–233.

(60) Kantor, Y.; Webman, I. Elastic properties of random percolating systems. *Phys. Rev. Lett.* **1984**, *52*, 1891–1894, DOI: 10.1103/PhysRevLett.52.1891.

(61) Kellomäki, M.; Aström, J.; Timonen, J. Rigidity and dynamics of random spring networks. *Phys. Rev. Lett.* **1996**, *77*, 2730–2733, DOI: 10.1103/PhysRevLett.77.2730.

(62) Moukarzel, C.; Duxbury, P. M. Comparison of rigidity and connectivity percolation in two dimensions. *Phys. Rev. E* **1999**, *59*, 2614–2622, DOI: 10.1103/PhysRevE.59.2614.

(63) Daoud, M. Viscoelasticity near the Sol-Gel Transition. *Macromolecules* **2000**, *33*, 3019–3022, DOI: 10.1021/ma991947s.

(64) Farago, O.; Kantor, Y. Entropic elasticity of phantom percolation networks. *Europhys. Lett.* **2000**, *52*, 413–419, DOI: 10.1209/epl/i2000-00453-y.

(65) Farago, O.; Kantor, Y. Entropic elasticity at the sol-gel transition. *Europhys. Lett.* **2002**, *57*, 458–463, DOI: 10.1209/epl/i2002-00482-6.

(66) Olasz, A.; Mignon, P.; Proft, F. D.; Veszprémi, T.; Geerlings, P. Effect of the π-π stacking interaction on the acidity of phenol. *Chem. Phys. Lett.* **2005**, *407*, 504–509, DOI: 10.1016/j.cplett.2005.03.145.

(67) Sanders, J. M. Optimal π-Stacking Interaction Energies in Parallel-Displaced Aryl/Aryl Dimers are Predicted by the Dimer Heavy Atom Count. *J. Phys. Chem. A* **2010**, *114*, 9205–9211, DOI: 10.1021/jp912094q.

Supporting Information Available

$$I_{nDQ} = \frac{I_{DQ}}{I_{REF} + I_{DQ}} \tag{SI.1}$$

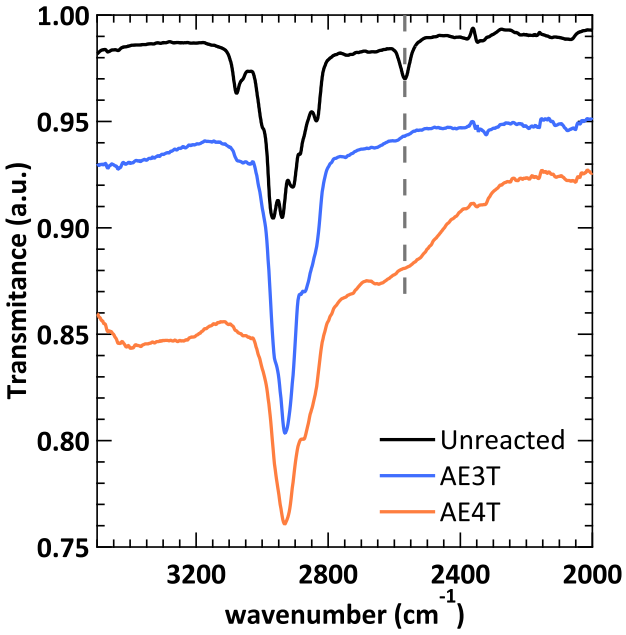

Figure SI.1: FT-IR spectra zoom-in for an unreacted medium and for the Neat *AE-3T* and *AE-4T* networks. Note the disappearance of the peak at 2568 cm^{-1} corresponding to the $-SH$ functions for the networks.

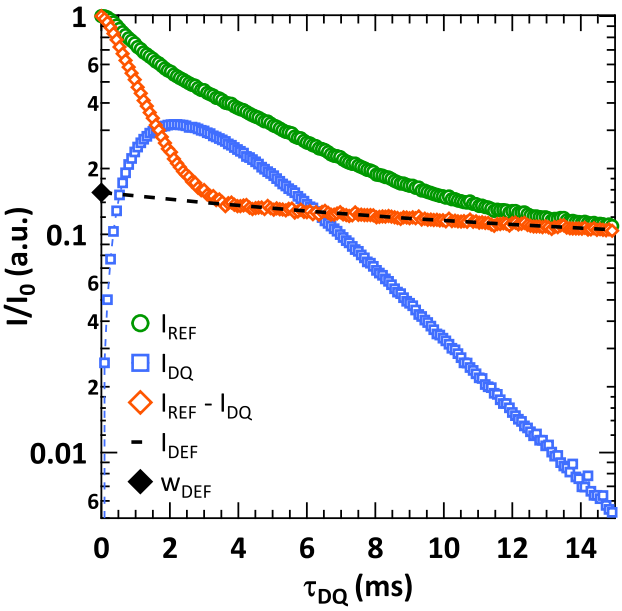

Figure SI.2: $DQ\,^1H$ NMR I_{ref}, I_{DQ}, $I_{ref}-I_{DQ}$, and I_{def} signals obtained for Neat *AE-3T* at T_α+140 °C. The contribution from defects I_{def} corresponds to the contribution from defects, with its fraction w_{def} being calculated by extrapolating I_{def} to $\tau_{DQ} = 0$.

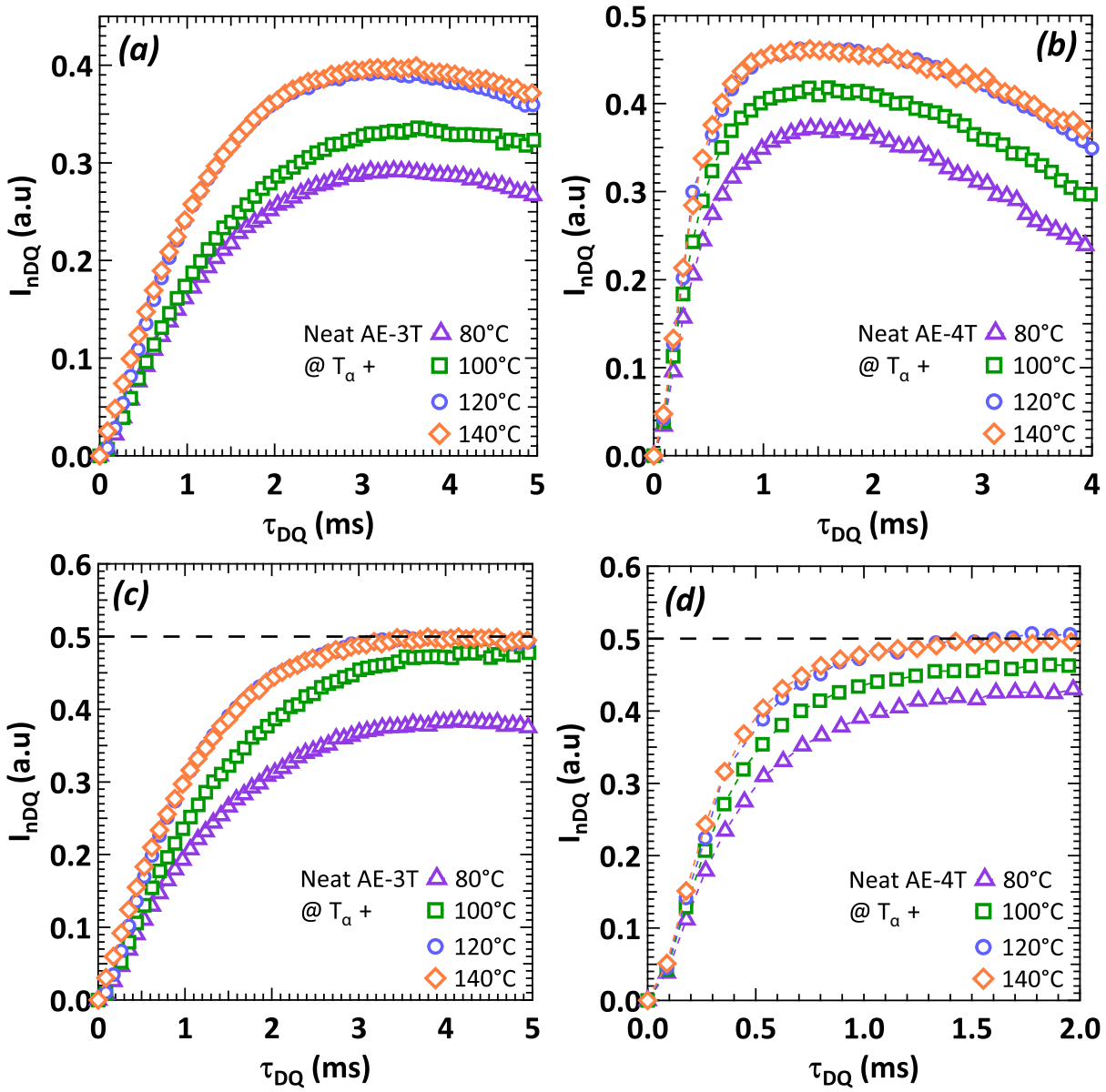

Figure SI.3: I_{nDQ} signals as a function of τ_{DQ} obtained by ^1H DQ-NMR normalized by Equation SI.1 (*Supporting Information*) for neat (a) *AE-3T* and (b) *AE-4T*, and normalized by Equation 5 for neat (c) *AE-3T* and (d) *AE-4T* networks at various $T + T_\alpha$ temperatures.

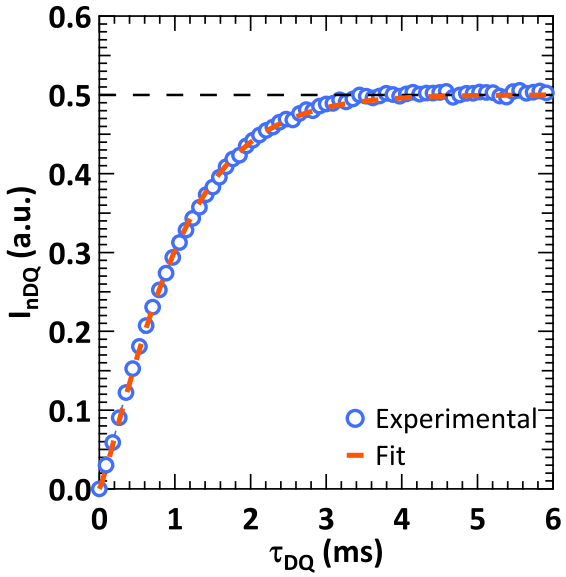

Figure SI.4: Normalized I_{nDQ} signal obtained for Neat *AE-3T* at T_α+140 °C according to Equation 5 and fitted by Equation 7.

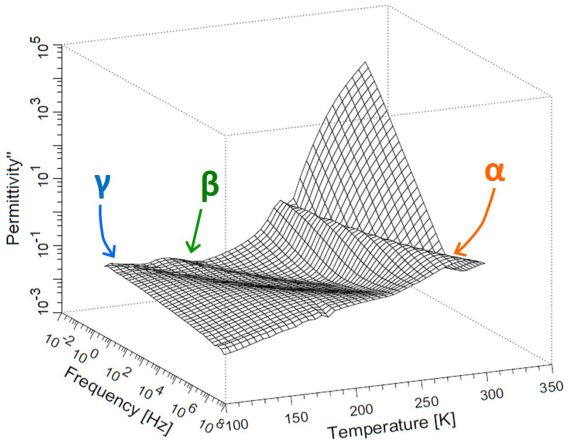

Figure SI.5: 3D spectrum of the loss dielectric permittivity ϵ'' as a function of frequency and temperature obtained by BDS measurements for the Neat *AE-3T* sample with highlighted secondary (γ and β) and main (α) molecular relaxations.

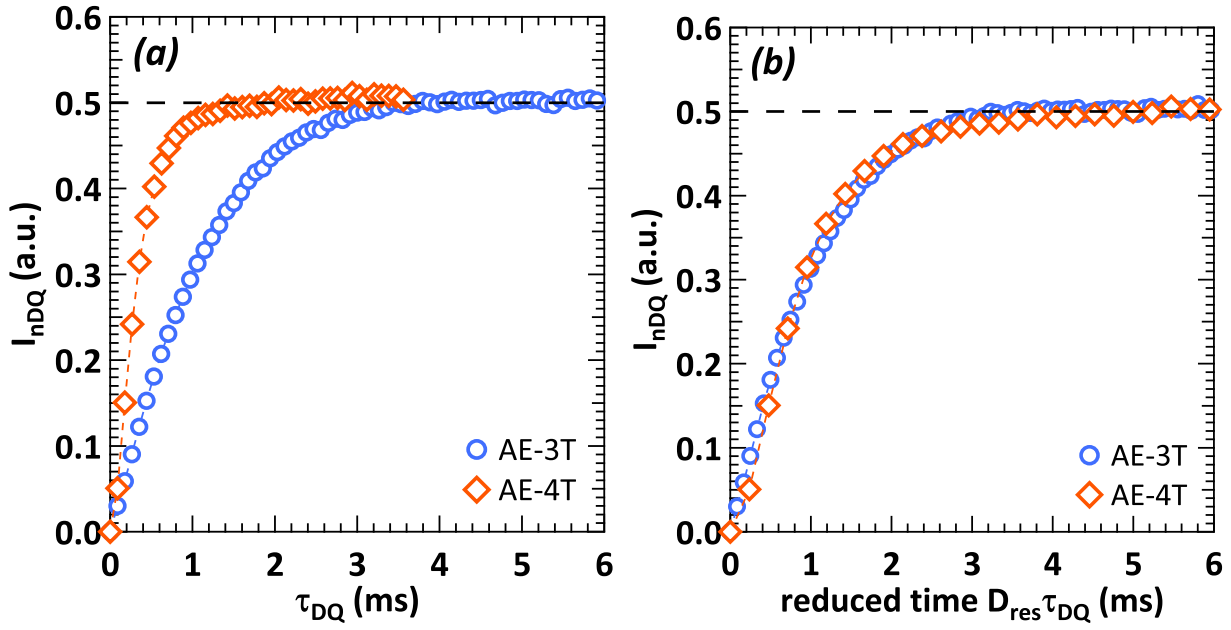

Figure SI.6: I_{nDQ} signals as a function of the DQ time (a) and (b) the normalized DQ time $D_{res}\tau_{DQ}$ obtained by ^1H DQ-NMR for Neat $AE\text{-}3T$ and $AE\text{-}4T$ at $T + T_\alpha$+140 °C.

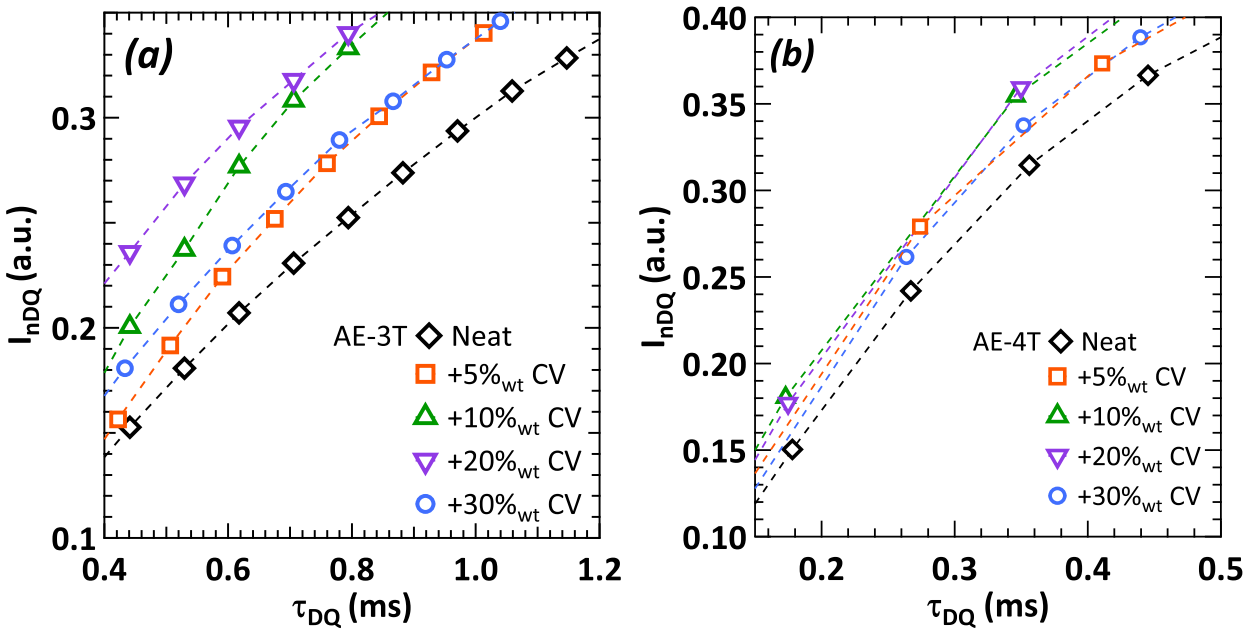

Figure SI.7: Zoom-ins of I_{nDQ} signals as a function of τ_{DQ} obtained by ^1H DQ-NMR for the (a) $AE\text{-}3T$ and (b) $AE\text{-}4T$ at $T + T_\alpha$+140 °C containing various percentages of CV.

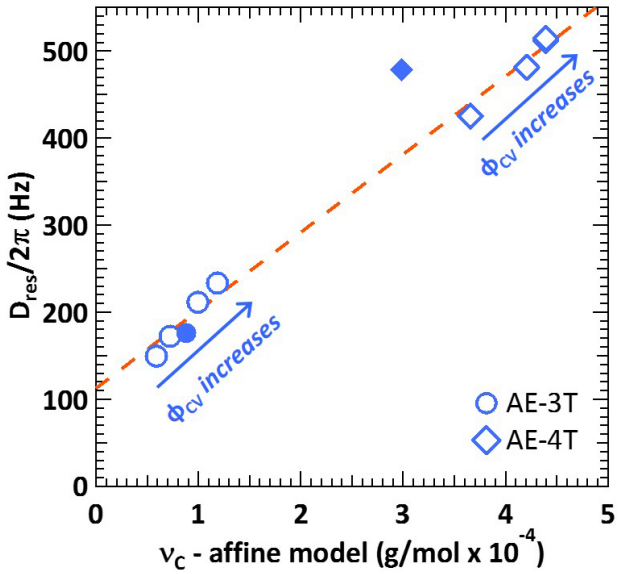

Figure SI.8: D_{res} obtained by ^1H *DQ*-NMR for the *AE-3T+CV* and *AE-4T+CV* samples as a function of the ν_C calculated from the affine model. The full markers correspond to the samples containing $30\%_{wt}$ *CV*. The dashed line is a linear fit and is a guide for the eyes.

Graphical TOC Entry